Shifts in stability and control effectiveness during evolution of the Paraves support aerial maneuvering hypotheses for flight origin

Dennis Evangelista [*] [†], **Sharlene Cam** [*], **Tony Huynh** [*], **Austin Kwong** [*], **Homayun Mehrabani** [*], **Kyle Tse** [*], **and Robert Dudley** [*] [‡]

[*]University of California, Berkeley, CA 94720-3140, United States of America,[†]current address University of North Carolina, Chapel Hill, NC 27510, United States of America, and [‡]Smithsonian Tropical Research Institute, Balboa, Panama

Submitted to Proceedings of the National Academy of Sciences of the United States of America

The capacity for aerial maneuvering shaped the evolution of flying animals. Here we evaluate consequences of paravian morphology for aerial performance [1, 2] by quantifying static stability and control effectiveness of physical models [3] for numerous taxa sampled from within the lineage leading to birds (Paraves, [4, 5]). Results of aerodynamic testing are mapped phylogenetically [6, 7, 8, 9, 10] to examine how maneuvering characteristics correlate with tail shortening, fore- and hindwing elaboration, and other morphological features. In the evolution of the Paraves we observe shifts from static stability to inherently unstable aerial planforms; control effectiveness also migrated from tails to the forewings. These shifts suggest that some degree of aerodynamic control and and capacity for maneuvering preceded the evolution of strong power stroke. The timing of shifts suggests features normally considered in light of development of a power stroke also play important roles in control.

stability | control effectiveness | maneuvering | flight evolution | Paraves

Abbreviations: COM, center of mass;3D, three-dimensional

Significance Statement: The dinosaurs that ultimately became birds possessed long, feathered tails and feathers on their legs along with feathers on their forelimbs, an arrangement unlike the tails of living birds. Both fore- and hindlimbs along with the tail would have served to control the animal in the air (like the tails on airplanes, except potentially at very steep flight angles), and by tracing out how aerodynamic control changed through time, we can examine how aerial maneuvering changed during paravian evolution.

Regardless of how aerial behavior originates, once airborne an organism must control [2] its orientation and position in order to safely navigate the vertical environment (e.g., directed aerial descent, [1]). Such abilities are present even in taxa with no obvious morphological adaptation for flight [11, 12, 13, 14]; at low speeds, such as at the start of a fall or jump, inertial mechanisms [15] allow for rolling, pitching, and yawing; as speeds increase (or as appendages grow in area), aerodynamic mechanisms of control can be employed. Body and appendage configuration position affect both stability, the tendency to resist perturbations, as well as production of torques and forces for maneuvering (control effectiveness). In the four-winged Early Cretaceous *Microraptor gui*, changes in planform, such as alternative reconstruction postures or removal of leg and tail feathers, alter stability and the control effectiveness of appendages [3]. Furthermore, appendage function can shift entirely according to the aerial environment (e.g. asymmetric wing pronation producing yaw at high glide angle versus roll at low glide angle) or even completely reverse function [3]. Such results are exciting but are based on a single specimen [16]. Stronger conclusions can be drawn from comparative study of several forms within a phylogenetic context.

One obvious trend in avian evolution is the transition from long tails and feathered legs in early forms [16, 17, 18, 19] to later (including extant) forms for which the skeletal tail has fused into a short pygostyle and both asymmetric and symmetric flight feathers are absent from the legs. Functional consequences of this shift remain speculative [20, 21, 22]. Similarly, changes in the pectoral girdle have been assumed to enhance a powered downstroke [5, 23], but may also have influenced maneuvering by shifting the center of body mass [24] or in enabling the production of wing asymmetries. With the exception of [25], previous studies tend to focus on lift and drag coefficients and glide angles and specific postures [26, 27, 28, 29], with maneuvering only considered rarely and in single taxa [18, 30, 3].

To examine these patterns and to test adaptive hypotheses [31], we can use model tests to quantify the effect of shape on stability and control effectiveness [3, 28, 32], using specimens sampled from early paravian [4] and avialan [5] evolution [7, 8, 9, 10]. We focus specifically on static stability and control effectiveness; while lift and drag are expected to be important in flight evolution, they have been addressed adequately in previous literature [3, 29, 28, 27]; while the capacity to generate aerodynamic forces was certainly present, we consider here the ability to control aerial behavior. We hypothesize that the presence or absence of stability in the various axes and the control effectiveness of the appendages should correlate with changes in major morphological features (shortening of the tail, enlargement of the forewings) to enhance aerodynamic performance. Alternatively, both stability and control may have been absent early in the evolution of flight, only appearing after a strong and bilaterally symmetric power stroke evolved.

Results and Discussion

Representative aerodynamic measurements for pitching stability and control effectiveness are given in Figure 1 for six paravians and one pterosaur. Tables of all aerodynamic measurements are provided in the Supporting Information. Long-tailed taxa (Figure 1A) show a stable equilibrium point and the tail is effective in generating pitching moments, whereas short-tailed taxa (Figure 1B) were unstable and had reduced control effectiveness of the tail. Notably, the same pattern (i.e., downward sloping C_m versus α) is seen consistently in two early representatives of the Avialaes, in a long-tailed pterosaur (*Rhamphorhynchus*), and in the paravian Early Cretaceous

Reserved for Publication Footnotes

dromaeosaur *Microraptor*, suggesting that these patterns more likely derive from shape and aerodynamics than from immediate ancestry.

All aerodynamic measurements were coded into both discretized and continuous character matrices (see Supporting Information), which were then mapped onto a phylogeny (assembled from [7, 8, 9, 10]) to examine the evolution of static stability and control effectiveness.

The study taxa show progressive tail loss as well as loss of leg-associated control surfaces along with a concomitant increase in forewing size and bony features associated with the pectoral girdle (nodes 1-4 on Figure 2). Changes in stability and control effectiveness here (as well as manipulations in which appendage surfaces were removed with all else held constant [3]) reflect these morphological changes. In pitch (Figure 2), taxa shift from being statically stable ancestrally to subsequently being unstable (and thus requiring active control). Control effectiveness concomitantly migrates from the ancestrally large and feathered tail and legs to the increasingly capable forewings, which become relatively larger, gain larger muscle attachments and gain skeletal features that improve production of fine left-right and fore-aft kinematic asymmetries needed for control.

Transition to forewing control correlates with elongation of the coracoid, along with other changes in the scapula (Figure 2, node 2). In addition, the sternum becomes successively modified within the Avialae [23], although a single shield-shaped sternum, more derived than *Archaeopteryx* is also seen in *Microraptor* [16]. Concomitantly, the tail becomes much reduced into a pygostyle (Figure 2, node 3). Other synapomorphies appear at node 4 (Figure 2), including the strut-like coracoid, triosseal canal, synsacrum and carinate sternum [23]. Whereas the latter features (node 4) feature in power production, the timing of the former features (nodes 2 and 3) appears consistent with enhanced forewing control effectiveness. Ontogenetic tests [33] show 4-day post hatching Chukar Partridge are capable of extreme maneuvers (rolling and pitching 180°) before strong development of a carinate sternum, suggesting this interpretation is correct.

In roll (Figure 3), taxa were stable at high angles of attack, but either unstable or marginally stable at low angles of attack; large asymmetric wing movements (i.e., wing tucking) were always effective in creating substantial rolling moments.

In yaw, all taxa at high angles of attack (Figure 4A) were marginally stable as might be expected from symmetry. Taxa with long tails were also stable at low angle-of-attack (Figure 4B), in agreement with computational results [34], but as tails are reduced, yaw stability becomes marginal and control migrates to the wings (as in pitch control). Asymmetric wing pronation and supination (Figures 4a and 4b) was effective in generating yawing moments in all taxa, suggesting maneuverability in yaw early in bird evolution. As the tail becomes shorter, flight becomes marginally stable or unstable, and control effectiveness must migrate (as in pitch control) from the shortening tail to the enlarging forewings. Stability in roll and in yaw shifts with angle of attack, which may serve as a proxy for glide angle or the steepness of descent. At high angles of attack, roll is the more stable axis, whereas stability in yaw is greater at low angles of attack. Forewing asymmetrical movements created substantial yawing moments in all taxa, whereas forewing symmetrical movements were only effective in later taxa.

The findings suggest that the capacity for maneuvering characterized the early stages of flight evolution [1], before forewings with a power stroke fully evolved. The large tail of early paravians yielded high aerodynamic control effectiveness and the body possessed some degree of stability. Combined with likely dynamic forces and torques generated by either tail whipping [15] or reduced amounts of asymmetric or symmetric forewing flapping, this suggests that the ancestral organisms were capable of controlled aerial behaviors at high angles of attack (Figures 2-4); the occasional presence of features often considered to be flight-related in other paravians, such as a shield-shaped sternum in *Microraptor* or long, robust forelimbs and modifications to the shoulder girdle early in the Paraves [4], supports the idea that maneuvering evolved in an incremental (vice quantum) way. Subsequent shifts in control would be consistent with more shallow glides facilitated by incipient wing flapping, which may have served initially in control but then ultimately became the power stroke characteristic of modern birds. Incipient flapping may thus have become elaborated as a control response [2] to instabilities demonstrated here. Body center of mass was migrating forward [24], but this is coupled with loss of long after surfaces and coincidence of the wing center with the COM. Active control was thus required as static stability was reduced and eventually lost, and associated forewing movements would also have enhanced aerodynamic force production and provided a means for inertial attitude adjustment. Once the transition to wing-mediated maneuverability and control began, larger surfaces and increased musculature would have facilitated dynamic force production for weight offset via the power stroke characteristic of modern birds.

Materials and Methods

Model construction. We constructed models (8 cm snout-vent length) of four extant birds, seven fossil paravians [4], encompassing five avialans [5], *Microraptor* [16] and *Anchiornis* [17], using 3D printing (Supporting Information, Figure S1). Fossils were selected to sample phylogenies available in 2011 (when the work was done), although an eighth paravian, *Zhongornis* [35], was later dropped due to questions about its phylogenetic position and because the specimen was identified to be a juvenile. To explore parallel evolution and for calibration, we also constructed models of three pterosaurs, two bats, and two artificial test objects (sphere and weather vane). Construction methods closely followed those of [28, 33, 11, 12]. Solid models were developed in Blender (The Blender Foundation, Amsterdam), closely referencing published photographs of fossils and reconstructions from the literature [17, 18, 36, 37, 38, 16, 39, 7] and casts of *Archaeopteryx* to match long bone, axial skeleton, and body proportions. Modeling was also guided by Starling dissections, preserved specimens, and vertebrate anatomy texts [23, 40].

Models were printed using a 3D printer (ProJet HD3000, 3D Systems, Rock Hill, SC), then mounted on 26-gauge steel armatures with felt or polymer clay filling in gaps between printed parts where flexibility was needed for repositioning. Wings were constructed using methods described in [28, 3]; wings were traced from published reconstructions, printed on paper and cut, with monofilament stiffening added along feather rachises and attached to 26-gauge steel limb and tail armatures (sized using scaled print outs of the fossils) using surgical tape (3M, St. Paul, MN). This procedure was found in previous work to match more laborious and less repeatable application of manually attached bird feathers [28]. The .STL files used to create the models are available for download to researchers wishing to replicate our models.

Body posture and appendage position. Fossil paravian models were reconstructed with wings spread and legs extended back [41, 3] (Figures 5 and 6). While alternative postures have been considered (specifically in *Microraptor* [16, 26, 42, 27, 43, 28, 44, 30, 3, 29], including some now considered infeasible), the aim of this study was to examine maneuvering within several species rather than the posture of one, and the legs-back posture is seen in extant birds as well as supported for the fossils [41, 42]. For control effectiveness, we tested fixed static appendage movements previously identified as being aerodynamically effective [3, 33]: asymmetric wing pronation and supination, wing tucking, symmetric wing protraction and retraction, and dorsoventral and lateral movements of the tail (Figure 6). The angular extent of each movement tested is shown on Figure 6.

Models were mounted at the estimated COM for the baseline body posture. The estimate was formed in Blender assuming a uniform density for the posed model, as in [24]. While we did duplicate the same sensitivity analyses as [24], we recognize that the COM estimate could vary up to 3-5% of the body length, or by smaller amounts for the variable load associated with appendage movements; this uncertainty is usually within the bounds of coefficient estimates identified as marginally stable.

Wind tunnel testing. Wind tunnel testing used previous methods [3], with a six-axis sensor (Nano17, ATI, Apex, NC) mounted to a 0.5 inch (12.7 mm) damped sting exiting the model downwind at the center of mass (Supplementary Fig.5). In some measurements, a 2 mm steel extension rod or a 3 mm acrylic plate were used to avoid geometric interferences and to keep the sting several diameters away and downstream of aerodynamic surfaces. The sensor was zeroed

for each measurement, eliminating deadweight effects. Models were tested in an open-circuit Eiffel-type wind tunnel with an 18×18×36-inch (45.7×45.7×91.4 cm) working section (Engineering Laboratory Design, Lake City, MN). Testing at 6 m s^{-1} resulted in a Reynolds number of ∼32,000 for all models, matching full scale for *Archaeopteryx*.

Under these conditions the aerodynamic coefficients of interest are reasonably constant with Re [3, 33]. Early in the evolution of animal flight, organisms likely flew at moderate speeds and high angles of attack [3, 29] where flows appear like bluff body turbulent flows (in which coefficients are largely independent of Re, for $10^3 < \text{Re} < 10^6$). In previous work [28, 3], we performed a sweep of wind tunnel speed, to examine Re from 30,000 to 70,000, to validate that scale effects were not present. As additional support for this approach, tests for maneuvering bodies are nearly always tested at well below full scale Re, e.g. the largest US Navy freely-maneuvering model tests are well below $\frac{1}{3}$-scale. Our methods were also previously benchmarked using model tests at full scale Re or gliding frogs [45, 32] (repeated for comparison), *Draco* lizards, Anna's Hummingbirds in glide and extreme dive pullout maneuvers, hummingbird body shapes in hovering [46], and reduced-scale tests of human skydivers compared to actual data [13, 14]; while at Re ~ 1000, our modeling methods have been benchmarked against extant winged seeds. Perching aerial robots, developed to test control algorithms, have shown good agreement between fully 3D robots and flat plate models with the same planform [47, 48, 49]. Results [3] for lift and drag coefficients using our method were agreed with those for full-scale *Microraptor* models in the other modeling tests [29, 27].

Sensor readings were recorded at 1000 Hz using a data acquisition card (National Instruments, Austin, TX) [3]. The sting was mounted to a servo (Hitec USA, Poway, CA) interfaced to a data acquisition computer, using an Arduino microcontroller (SparkFun, Boulder, CO) and specially written code in Python and R [50], to automate positioning and measurement of windspeed and force/torque. Raw measurements were rotated to a frame aligned with the wind tunnel and flow using the combined roll, pitch, and yaw angles by multiplication with three Euler rotation matrices; translation from the sensor to the model COM was also included. Transformed measurements were averaged over a one-minute recording. We then computed non-dimensional force and moment coefficients, static stability coefficients, and control effectiveness [32, 3, 51]. Three series, varying pitch, roll, and yaw, were conducted at 5° increments. Using the automatic sting, we obtained 13,792 measurements, with at least five replicates for 18 models in 247 total positions: generally 5 each in pitch (88 total), 2 each in roll for two angles of attack (69 total), and 3 each in yaw for two angles of attack (92 total). Test positions are indicated on Figure 6.

Static stability was measured by examining the sign of the slope $\partial C_m/\partial\alpha$ (positive slope is unstable, negative stable, zero marginally stable, see Figures 5C) of the non-dimensional pitching moment coefficient C_m near fixed points as the body was subjected to small deflections $d\alpha$ [3, 32, 51]:

$$\text{pitching moment } M = 0.5\rho U^2 C_m \lambda S \qquad \textbf{[1]}$$

Control effectiveness ($\partial C_m/\partial\delta$, [52, 32, 3]) was measured by deflecting appendages (Figure 6) by an amount $d\delta$ and examining the change in pitching moment coefficient. Both are unitless (rad^{-1}). A first-order estimate of maneuvering is obtained from considering the two together and a biomechanical trade-off is apparent: a stable object can resist perturbations from the environment with minimal control effort but will also have difficulty in changing direction (which might be necessary to accomplish aerial righting, navigate in cluttered forests, seek resources or avoid predators). The metrics underestimate maneuvering in very dynamic cases (high advance ratio flapping or where second-order damping terms become important [53]), but are adequate for quasi-static maneuvers. Locomotion is a complex task, and passive stability is often exploited where possible to reduce control effort; conversely, passive instability may be exploited in extreme (and likely elective) maneuvers. The absence of stability, coupled with the presence of large control effectiveness, could be used to infer the presence of strong closed-loop neuromuscular control. The absence of control effectiveness suggests a lack of control, as even with feedback an ineffective surface cannot generate the necessary forces and torques. Thus, while the full control abilities of an extinct form are difficult if not impossible to fully enumerate, the simple metrics here provide a useful proxy.

Phylogenetic comparisons. A Nexus file without branch lengths, available in the Supplementary Material, was assembled from published phylogenies [7, 8, 9, 10] of the study taxa. While revisions to the phylogenetic relationships have been discussed [4, 54], they do not appear to alter the patterns in stability and control effectiveness; trees from [4, 54] are included in the Nexus file. Mapping of discrete maneuvering traits was performed in Mesquite [6] with the built-in ancestral state reconstruction routines using unordered parsimony. Aerodynamic measurements were coded into a matrix giving eight discretized stability values (stable, marginal, unstable); ten discrete morphological traits drawn from [23, 16, 17, 18, 36, 37, 38, 39, 7] (also shown on Figure 2 as nodes 1-4), and 12 discretized control effectiveness values. The discretized control effectiveness values were obtained from the measurements by thresholding based on the moment necessary to overcome measured weather vane stability, or equivalently, to cause a displacement of the center of aerodynamic pressure of about 10% of total length.

ACKNOWLEDGMENTS. We thank Y. Munk, Y. Zeng, E. Kim, M. Wolf, N. Sapir, V. Ortega, S. Werning, K. Peterson, J. McGuire and R. Fearing for their advice and assistance. We than the Berkeley Undergraduate Research Apprentice Program (URAP) and the help of G. Cardona, C. Chun, M. Cohen, E. Guenther-Gleason, V. Howard, S. Jaini, F. Linn, C. Lopez, A. Lowenstein, D. Manohara, D. Marks, N. Ray, A. Tisbe, F. Wong, O. Yu and R. Zhu. The manuscript was improved using comments from 5 anonymous reviewers. DE was supported by an NSF Minority Graduate Research Fellowship, UC Chancellor's Fellowship, and NSF Integrative Graduate Education and Research Traineeship (IGERT) #DGE-0903711. TH was supported by the University of California Museum of Palaeontology (UCMP). We also thank T. Libby and the Berkeley Center for Integrative Biomechanics in Education and Research (CIBER) for use of a force sensor and 3D printer.

1. **Dudley R, Yanoviak S (2011) Animal aloft: the origins of aerial behavior and flight. *Integr. Comp. Biol.* 51:926–936.**
2. **Smith JM (1952) The importance of the nervous system in the evolution of animal flight. *Evolution* 6:127–129.**
3. **Evangelista D et al. (2014) Aerodynamic characteristics of a feathered dinosaur measured using physical models. effects of form on static stability and control effectiveness. *PLoS ONE* 9.**
4. **Xu X, You H, Du K, Han F (2011) An *Archaeopteryx*-like theropod from China and the origin of Avialae. *Nature* 475:465–70.**
5. **Gauthier J, Padian K (1985) in *Beginnings of the Birds: Proceedings of the International Archaeopteryx Conference*, eds. Hecht M, Ostrom J, Viohl G, Wellnhover P. (Freunde des Jura-Museums), pp. 185–197.**
6. **Maddison WP, Maddison DR (2010) *Mesquite: A modular system for evolutionary analysis*.**
7. **Zhou Z, Li FZZ (2010) A new Lower Cretaceous bird from China and tooth reduction in early avian evolution. *Proc. R. Soc. B.* 277:219–227.**
8. **Li Q et al. (2010) Plumage color patterns of an extinct dinosaur. *Science* 327:1369–1372.**
9. **O'Connor J, Chiappe LM, Bell A (2011) in *Living Dinosaur: Evolutionary History of the Modern Birds*, eds. Dyke G, Kaiser G. (John Wiley & Sons), pp. 39–105.**
10. **Cracraft J et al. (2004) in *Assembling the Tree of Life*, eds. Cracraft J, Donoghue MJ. (Oxford University Press), pp. 468–489.**
11. **Munk JD (2011) Ph.D. thesis (University of California, Berkeley).**
12. **Zeng Y (2013) Ph.D. thesis (University of California, Berkeley).**
13. **Cardona G, Evangelista D, Ray N, Tse K, Wong D (2011) Measurement of the aerodynamic stability and control effectiveness of human skydivers. *American Society of Biomechanics Annual Meeting, Long Beach, CA*.**
14. **Evangelista D, Cardona G, Ray N, Tse K, Wong D (2012) Measurement of the aerodynamic stability and control effectiveness of human skydivers during free fall and directed aerial descent. *Integrative and Comparative Biology* 52:E54.**
15. **Jusufi A, Goldman DI, Revzen S, Full RJ (2008) Active tails enhance arboreal acrobatics in geckos. *Proceedings of the National Academy of Sciences of the United States of America* 105:4215–4219.**
16. **Xu X et al. (2003) Four-winged dinosaurs from China. *Nature* 421:335–340.**
17. **Hu D, Hou L, Zhang L, Xu X (2009) A pre-Archaeopteryx troodontid theropod from China with long feathers on the metatarsus. *Nature* 461:640–6433.**
18. **Longrich N (2006) Structure and function of hindlimb feathers in *Archaeopteryx lithographica*. *Paleobiology* 32:417–431.**
19. **Christiansen P, Bonde N (2004) Body plumage in *Archaeopteryx*: a review, and new evidence from the Berlin specimen. *Comptes Rendus Palevol* 3:99–118.**
20. **Smith JM (1953) Birds as aeroplanes. *New Biology* 14:64–81.**
21. **Beebe CW (1915) A tetrapteryx stage in the ancestry of birds. *Zoologica* 2:39–52.**
22. **Thomas ALR (1997) On the tails of birds. *Bioscience* 47:215–225.**
23. **Benton MJ (2005) *Vertebrate Paleontology*. (Blackwell Publishing).**
24. **Allen V, Bates KT, Li Z, Hutchinson JR (2013) Linking the evolution of body shape and locomotor biomechanics in bird-line archosaurs. *Nature* 497:104–107.**
25. **Huynh T, Chun C, Evangelista D, Kwong A, Tse K (2011) Aerodynamic characteristics of feathered dinosaur shapes measured using physical models: A comparative study of maneuvering. *Journal of Vertebrate Paleontology* 31:129.**

26. Chatterjee S, Templin RJ (2007) Biplane wing planform and flight performance of the feathered dinosaur *Microraptor gui. Proc. Nat. Acad. Sci. USA* 104:1576–1580.
27. Alexander DE, Gong E, Martin LD, Burnham DA, Falk AR (2010) Model tests of gliding with different hindwing configurations in the four-winged dromaeosaurid *Microraptor gui. Proc. Nat. Acad. Sci. USA* 107:2972–2976.
28. Koehl MAR, Evangelista D, Yang K (2011) Using physical models to study the gliding performance of extinct animals. *Integrative and Comparative Biology* 51:1002–1018.
29. Dyke G et al. (2013) Aerodynamic performance of the feathered dinsoaur *Microraptor* and the evolution of feathered flight. *Nature Communications* 4:2489.
30. Hall J, Habib M, Hone D, Chiappe L (2012) A new model for hindwing funtion in the four-winged theropod dinosaur *Microraptor gui. Society of Vertebrate Paleontology Annual Meeting, Raleigh, NC.*
31. Padian K (2001) Cross-testing adaptive hypotheses: Phylogenetic analysis and the origin of bird flight. *Amer. Zool.* 41:598–607.
32. McCay MG (2001) Aerodynamic stability and maneuverability of the gliding frog *Polypedates dennysi. Journal of Experimental Biology* 204:2826–2917.
33. Evangelista DJ (2013) Ph.D. thesis (UC Berkeley).
34. Sachs G (2007) Tail effects on yaw stability in birds. *Journal of Theoretical Biology* 249:464–472.
35. Gao C et al. (2008) A new basal lineage of early Cretaceous birds from China and its implications on the evolution of the avian tail. *Paleontology* 51:775–791.
36. Hou Lh, Zhou Z, Martin LD, Feduccia A (1995) A beaked bird from the Jurassic of China. *Nature* 377:616–618.
37. Zhou Z, Zhang F, Science B (2002) A long-tailed, seed-eating bird from the early Cretaceous of China. *Nature* 418:405–409.
38. Zhou Z, Zhang F (2003) *Jeholornis* compared to *Archaeopteryx*, with a new understanding of the earliest avian evolution. *Die Naturwissenschaften* 90:220–5.
39. Zhou Z, Zhang F (2003) Anatomy of the primitive bird *Sapeornis chaoyangensis* from the Early Cretaceous of Liaoning, China. *Canadian Journal of Earth Sciences* 40:731–747.
40. Liem K, Bemis W, Walker W, Grande L (2000) *Functional Anatomy of the Vertebrates: An Evolutionary Perspective.* (Cengage Learning), 3rd edition.
41. Xu X, Zhou Z, Zhang F, Wang X, Kuang XW (2004) Functional hind-wings conform to the hip-structure in dromaeosaurids. *Journal of Vertebrate Paleontology* 24:251A.
42. Davis M (2008) Four winged dinosaur (NOVA television broadcast on PBS, February 26, 2008).
43. Hone DWE, Tischlinger H, Xu X, Zhang F (2010) The extent of the preserved feathers on the four-winged dinosaur *Microraptor gui* under ultraviolet light. *PLoS One* 5:e9223.
44. Habib M, Hall J, Hone D, Chiappe L (2012) Aerodynamics of the tail in *Microraptor* and the evolution of theropod flight control. *Society of Vertebrate Paleontology Annual Meeting, Raleigh, NC.*
45. Emerson SB, Travis J, Koehl MAR (1990) Functional complexes and additivity in performance: a test case with "flying" frogs. *Evolution* 44:2153–2157.
46. Sapir N, Dudley R (2012) Backward flight in hummingbirds employs unique kinematic adjustments and entails low metabolic costs. *J exp Biol* 215:3603–3611.
47. Roberts JW, Cory R, Tedrake R (2009) On the controllability of fixed-wing perching. *American Control Conference* pp. 2018–2023.
48. Hoburg W, Tedrake R (2009) System identification of post stall aerodynamics for UAV perching. *AIAA Infotech.*
49. Tangler J, Kucurek JD (2005) Wind turbine post-stall airfoil performance characteristics guidelines for blade-element momentum methods. *43rd AIAA Aerospace Sciences Meeting.*
50. R Core Team (2014) *R: A Language and Environment for Statistical Computing* (R Foundation for Statistical Computing, Vienna, Austria).
51. McCormick BW (1995) *Aerodynamics, Aeronautics and Flight Mechanics.* (John Wiley and Sons), 2nd edition.
52. Etkin B, Reid LD (1996) *Dynamics of Flight: Stability and Control.* (John Wiley and Sons, Inc., New York), 3rd edition.
53. Sachs G (2005) Yaw stability in gliding birds. *J Ornithol* 146:191–199.
54. Godefroit P, Cau A, H DY, Escuillié F, Wu WH (2013) A Jurassic avialan dinosaur from China resovles the early phylogenetic history of birds. *Nature* 498:359–362.

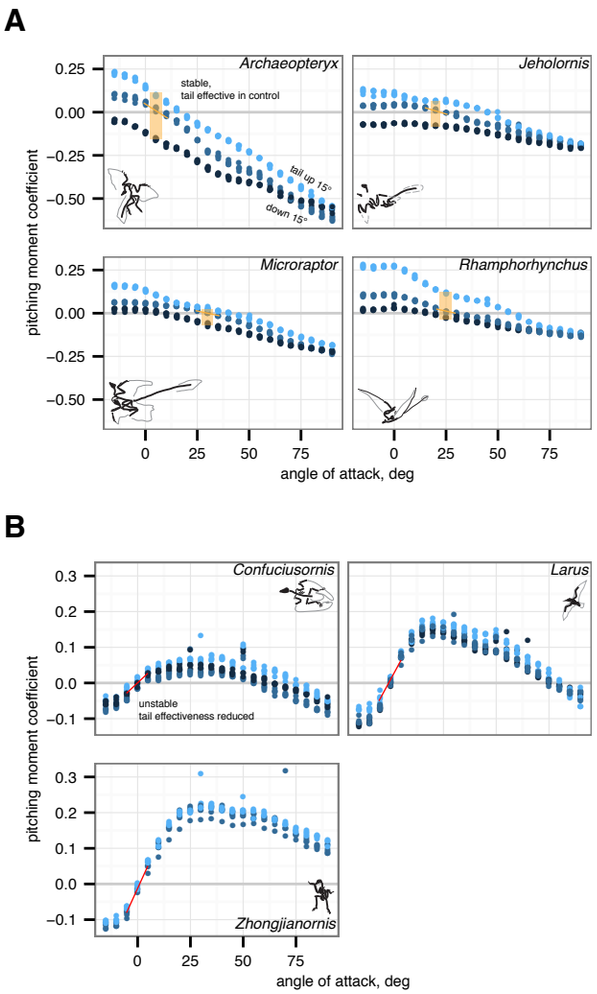

Fig. 1. Representative aerodynamic measurements for pitching stability and control effectiveness. Long-tailed taxa (A) have a stable equilibrium point at 10-25° (yellow line) and the tail is effective in generating pitching moments at low angles of attack (pale yellow box). In short-tailed taxa (B), including extant *Larus*, the equilibrium point at 0-5° is unstable (red line) and the tail control effectiveness is reduced. One example (*Rhamphorhynchus*) drawn from pterosaurs illustrates similar possibilities in a phylogenetically distant taxon.

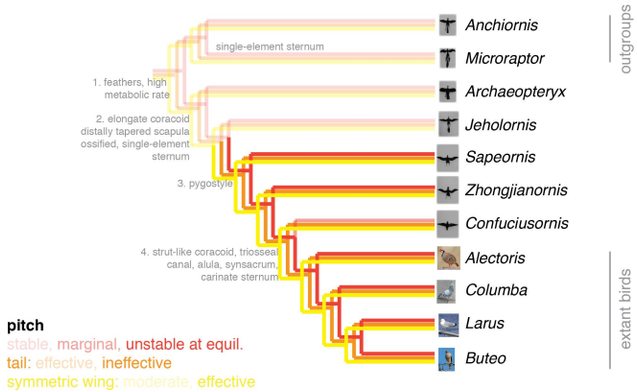

Fig. 2. Evolution of pitch stability and control effectiveness. Pitching stability is plotted in red hues, indicating stable (pale), marginally stable (medium), and unstable (solid). Control effectiveness of the tail in generating pitching moments is plotted in orange hues, indicating large control effectiveness (pale) or reduced control effectiveness (solid). Control effectiveness of symmetric wing protraction/retraction is plotted in yellow hues indicating large (pale) or reduced (solid). Consilience among the three traits indicates that early in the evolution of the Paraves, taxa are stable with a large degree of pitch control from the tail; later taxa are unstable, and control has migrated from the now reduced tail, to the wings, which become larger and develop skeletal features that would enhance control and the production of left-right and fore-aft asymmetries. Nodes 1-4 identify other skeletal features (reviewed in [23] and discussed in relation to the aerodynamic characters in the text.

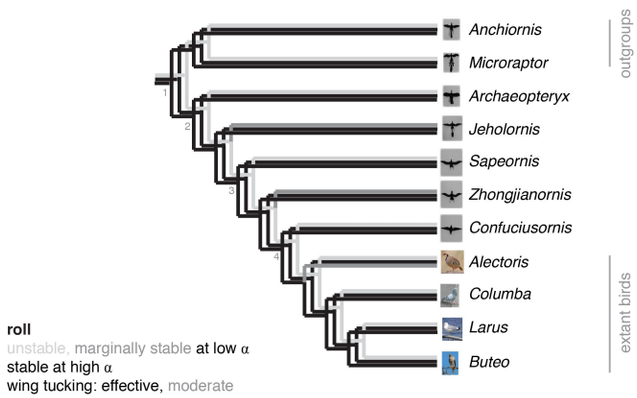

Fig. 3. Evolution of roll stability and control effectiveness. Characters shown are stability at low angle of attack (mostly unstable due to symmetry; *Sapeornis* marginal); stability at high angles of attack (all stable); and control effectiveness of asymmetric wing tucking in roll (always effective). As animals developed the ability to fly at reduced body angles of attack, more active control of roll would have been necessary, at first perhaps using inertial modes of the tail, but subsequently augmented with the forewings.

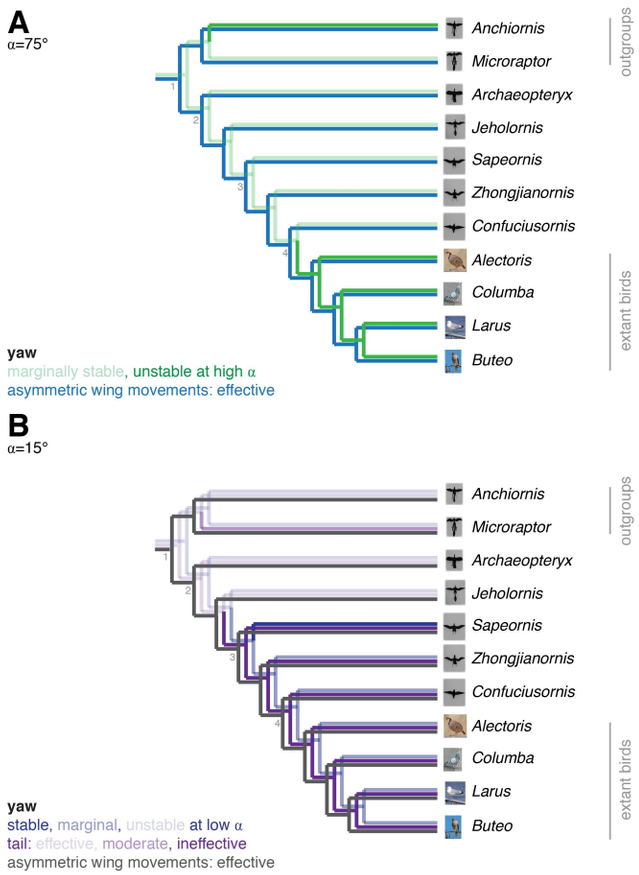

Fig. 4. Evolution of yaw stability and control effectiveness. At high angles of attack (A), taxa are mostly marginally stable as might be expected from symmetry. Asymmetric pronation and supination of the wings are always effective in generating yaw at high angles of attack. At reduced angles of attack (B), by contrast, long-tailed taxa are stable and can control yaw with the tail. As tails reduce in size, taxa become unstable in yaw at low angles of attack and lose the ability to control yaw with the tail. However, asymmetric movements of the wings are effective in producing yaw throughout the evolution of this clade, and control would thus have shifted from the tail to the forewings paralleling the shifts seen in pitch.

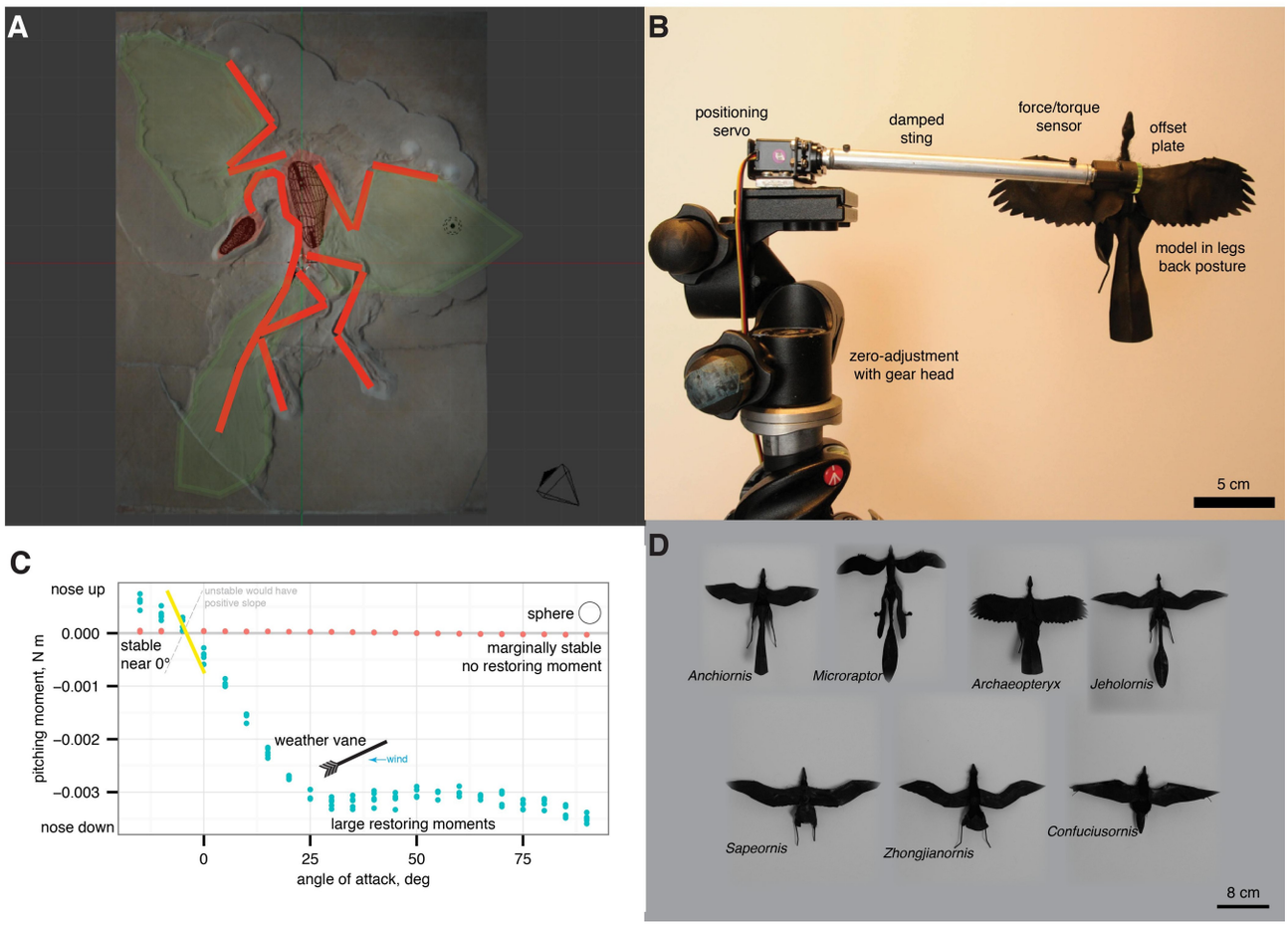

Fig. 5. Model construction, testing, and measurement of moments. Models were developed in Blender (A) from fossils (*Archaeopteryx* shown) and constructed and tested (B) using previous methods [32, 28, 3]. For simple cases such as a sphere or a weather vane, the relationship between slope and stability (C) is observed by plotting pitching moments versus angle-of-attack. Moments for sphere are not statistically different than zero, indicating marginal stability as expected. Models for fossil paravians studied are shown in (D).

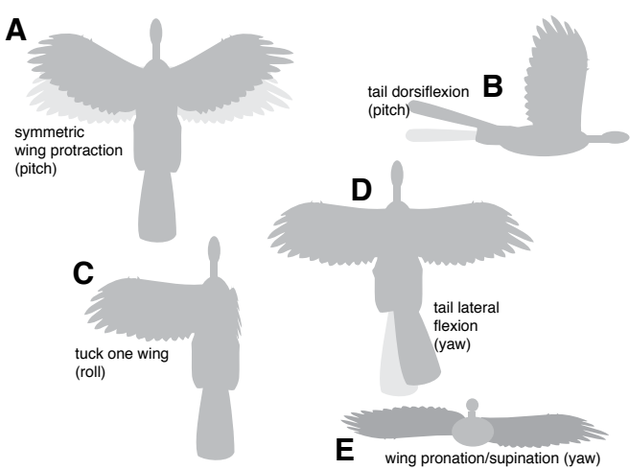

Fig. 6. Appendage movements tested to determine control effectiveness. Appendage movements were selected based on those observed to be effective in previous work [3], including (A) symmetric wing protraction (e.g. wing sweep to $\pm 45°$); (B) tail dorsiflexion to $\pm 15°$; (C) tucking of one wing; (D) tail lateral flexion to $30°$; and (E) asymmetric wing pronation/supination to ^{circ}.

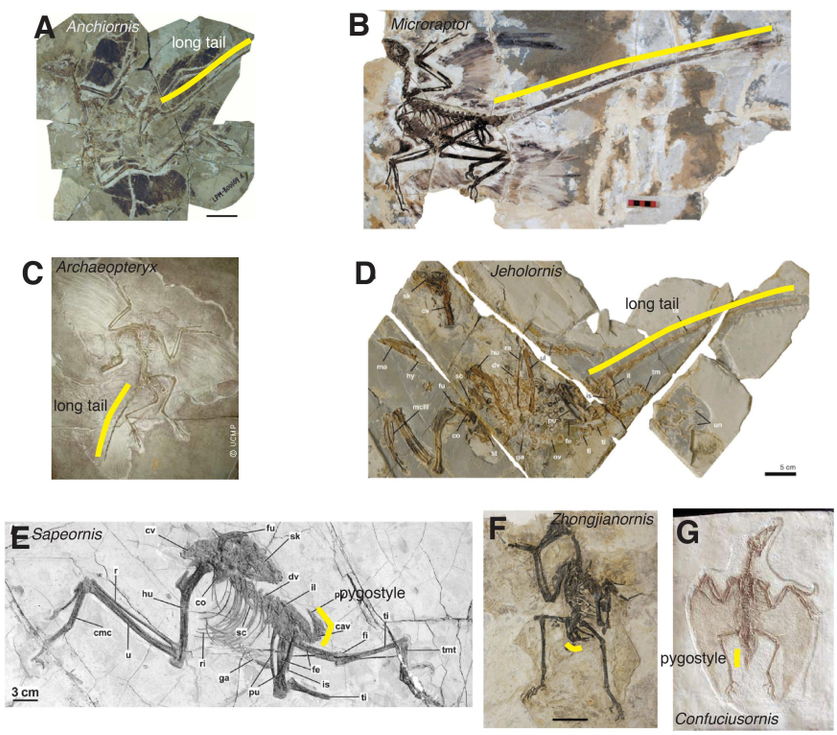

Fig. S1. Fossils paravians [4] used for comparative study. (A) *Anchiornis* [17]; (B) *Microraptor* [16]; (C) *Archaeopteryx* [23, 18], (D) *Jeholornis* [37, 38], (E) *Sapeornis* [38], (F) *Zhongjianornis* [7] and (G) *Confuciusornis* [35, 36]

Table S1. (A) Pitch static stability and equilibrium point, (B) control effectiveness in pitch using tail dorsiflexion (Figure 6B), (C) control effectiveness in pitch using symmetric wing protraction/retraction (wing sweep, Figure 6A). Results give mean ± s.d., $n = 15$ for stability, $n = 5$ for control effectiveness; units for stability and control effectiveness are rad^{-1}.

	pitch stability, $dC_m/d\alpha$			equilibrium point	
	$\alpha = 0°$	$\alpha = 15°$	$\alpha = 75°$	$\alpha°$	equilibrium $dC_m/d\alpha$
Anchiornis	-0.005 ±0.013	-0.067 ±0.012	-0.13 ±0.03	29 ± 2	-0.170 ±0.028
Archaeopteryx	-0.134 ±0.013	-0.221 ±0.020	-0.18 ±0.03	9 ± 2	-0.190 ±0.012
Confuciusornis	0.142 ±0.009	0.039 ±0.020	-0.06 ±0.02	0 ±2	-0.030 ±0.073
Jeholornis	0.011 ±0.018	-0.108 ±0.010	-0.10 ±0.02	25 ±1	-0.120 ±0.044
Microraptor	-0.039 ±0.006	-0.071 ±0.009	-0.17 ±0.02	20 ± 2	-0.070 ±0.029
Sapeornis	0.109 ±0.010	0.007 ±0.011	-0.11 ±0.02	5 ± 2	0.100 ±0.052
Zhongjianornis	0.305 ±0.036	0.195 ±0.027	-0.15 ±0.16	5 ±1	0.180 ±0.078
Alectoris	0.206 ±0.006	0.090 ±0.020	-0.37 ±0.16	0 ± 1	0.120 ±0.013
Buteo	0.187 ±0.010	-0.042 ±0.009	-0.13 ±0.02	0 ± 3	0.140 ±0.030
Columba	0.046 ±0.014	-0.047 ±0.017	-0.18 ±0.16	0 ± 6	0.050 ±0.088
Larus	0.352 ±0.028	0.092 ±0.015	-0.10 ±0.02	0 ± 1	0.150 ±0.049
Onychonycteris	-0.011 ±0.011	-0.112 ±0.005	-0.12 ±0.02	10 ± 2	-0.011 ±0.033
Pteropus	-0.118 ±0.014	-0.055 ±0.008	-0.10 ±0.02	0 ± 2	-0.080 ±0.015
Pteranodon	0.054 ±0.023	0.004 ±0.018	-0.07 ±0.04	5 ± 3	-0.050 ±0.029
Pterodactylus	-0.020 ±0.020	-0.050 ±0.009	-0.05 ±0.03	0 ± 4	-0.040 ±0.009
Rhamphorhynchus	-0.062 ±0.013	-0.192 ±0.024	-0.05 ±0.01	15 ± 1	-0.180 ±0.044
Sphere	-0.037 ±0.023	-0.020 ±0.022	-0.03 ±0.01		-0.050 ±0.006
Weathervane	-0.333 ±0.040	-0.347 ±0.020	-0.03 ±0.04	0 ± 2	-0.210 ±0.055

	$dC_m/d\delta$, tail dorsiflexion *			$dC_m/d\delta$, sym protraction / wing sweep †		
	$\alpha = 0°$	$\alpha = 15°$	$\alpha = 75°$	$\alpha = 0°$	$\alpha = 15°$	$\alpha = 75°$
Anchiornis	0.168 ±0.002	0.191 ±0.006	0.047 ±0.012	0.00±0.020	0.050±0.020	0.070 ±0.004
Archaeopteryx	0.219 ±0.007	0.190 ±0.010	0.065 ±0.024	-0.003 ±0.016	0.060 ±0.018	0.128 ±0.004
Confuciusornis	0.011 ±0.003	0.013 ±0.003	0.018 ±0.005	0.006 ±0.034	0.117 ±0.023	0.229 ±0.002
Jeholornis	0.268 ±0.019	0.223 ±0.001	0.068 ±0.005	0.042 ±0.009	0.072 ±0.006	0.088 ±0.002
Microraptor	0.174 ±0.023	0.125 ±0.002	0.089 ±0.014	0.018 ±0.008	0.037 ±0.003	0.051 ±0.004
Sapeornis	0.054 ±0.001	0.064 ±0.005	0.082 ±0.006	0.022 ±0.038	0.173 ±0.039	0.329 ±0.001
Zhongjianornis	0.023 ±0.004	0.019 ±0.004	0.012 ±0.026	0.025 ±0.027	0.119 ±0.023	0.221 ±0.001
Alectoris	0.011 ±0.004	0.012 ±0.005	0.044 ±0.007	-0.001 ±0.017	0.124 ±0.020	0.119 ±0.002
Buteo	0.018 ±0.003	0.033 ±0.012	0.049 ±0.006	0.043 ±0.034	0.142 ±0.021	0.213 ±0.001
Columba	0.044 ±0.004	0.050 ±0.003	0.009 ±0.002	0.076 ±0.027	0.151 ±0.013	0.168 ±0.002
Larus	0.014 ±0.008	0.016 ±0.003	0.014 ±0.008	-0.007 ±0.030	0.110 ±0.032	0.231 ±0.001
Onychonycteris	0.029 ± 0.004	0.032 ± 0.002	0.004 ± 0.004	0.031 ±0.030	0.152 ±0.031	0.235 ±0.003
Pteropus	0.053 ± 0.009	0.026 ± 0.003	0.026 ± 0.002	-0.005 ±0.041	0.131 ±0.030	0.230 ±0.002
Pteranodon	0.016 ±0.005	0.015 ±0.002	0.016 ±0.003	0.167 ±0.050	0.315 ±0.033	0.480 ±0.001
Pterodactylus	0.015 ±0.002	0.025 ±0.004	0.039 ±0.005	0.005 ±0.026	0.088 ±0.018	0.141 ±0.002
Rhamphorhynchus	0.347 ±0.016	0.245 ±0.032	0.029 ±0.010	0.012 ±0.025	0.045 ±0.020	0.175 ±0.001

*movement depicted in Figure 6B

†movement depicted in Figure 6A

Table S2. (A) Roll static stability and (B) control effectiveness in roll for asymmetric wing tucking (Figure 6C). Results give mean $\pm$ s.d. for $n = 15$; units for stability and control effectiveness are rad^{-1}. Equilibrium point in roll is at $\phi = 0°$.

	A		B	
	roll stability, $dC_r/d\phi$		$dC_r/d\delta$, asymmetric wing tuck *	
	$\alpha = 15°$	$\alpha = 75°$	$\alpha = 15°$	$\alpha = 75°$
Anchiornis				
Archaeopteryx	0.009 $\pm$ 0.06	-0.200 $\pm$ 0.019	0.090 $\pm$ 0.005	0.200 $\pm$ 0.018
Confuciusornis	-0.020 $\pm$ 0.02	-0.200 $\pm$ 0.009	0.050 $\pm$ 0.002	0.100 $\pm$ 0.012
Jeholornis	0.073 $\pm$ 0.03	-0.400 $\pm$ 0.025	0.080 $\pm$ 0.004	0.120 $\pm$ 0.024
Microraptor	0.132 $\pm$ 0.03	-0.300 $\pm$ 0.019	0.050 $\pm$ 0.007	0.170 $\pm$ 0.021
Sapeornis	0.043 $\pm$ 0.04	-0.300 $\pm$ 0.026	0.080 $\pm$ 0.002	0.130 $\pm$ 0.016
Zhongjianornis	0.030 $\pm$ 0.02	-0.200 $\pm$ 0.012	0.050 $\pm$ 0.001	0.140 $\pm$ 0.015
Alectoris	0.009 $\pm$ 0.06	-0.100 $\pm$ 0.016	0.060 $\pm$ 0.002	0.080 $\pm$ 0.007
Buteo	0.028 $\pm$ 0.05	-0.400 $\pm$ 0.022	0.170 $\pm$ 0.012	0.240 $\pm$ 0.055
Columba	-0.030 $\pm$ 0.05	-0.300 $\pm$ 0.014	0.180 $\pm$ 0.007	0.180 $\pm$ 0.027
Larus	-0.009 $\pm$ 0.02	-0.400 $\pm$ 0.028	0.150 $\pm$ 0.004	0.200 $\pm$ 0.038
Onychonycteris		-1.000 $\pm$ 0.044	0.810 $\pm$ 0.036	0.880 $\pm$ 0.100
Pteropus	-0.027 $\pm$ 0.05	-0.700 $\pm$ 0.064	0.680 $\pm$ 0.020	0.830 $\pm$ 0.088
Pteranodon	0.011 $\pm$ 0.02	-0.200 $\pm$ 0.014	0.070 $\pm$ 0.002	0.100 $\pm$ 0.010
Pterodactylus	-0.002 $\pm$ 0.06	-0.300 $\pm$ 0.016	0.100 $\pm$ 0.003	0.110 $\pm$ 0.027
Rhamphorhynchus	-0.069 $\pm$ 0.03	-0.400 $\pm$ 0.021	0.160 $\pm$ 0.007	0.210 $\pm$ 0.030

*movement depicted in Figure 6C

Table S3. (A) Yaw static stability, (B) control effectivenes in yaw using tail lateral flexion (Figure 6D), (C) control effectiveness in yaw using wing pronation/supination (Figure 6E), (D) control effectiveness in yaw using lateral head flexion for pterosaurs only. Results give mean $\pm$ s.d., $n = 15$ for stability, $n = 5$ for control effectiveness; units for stability and control effectiveness are rad^{-1}. Equilibrium point in yaw is at $\psi = 0°$.

	A		B		C		D	
	yaw stability, $dC_y/d\psi$		$dC_y/d\delta$, lateral tail flexion *		$dC_y/d\delta$, wing pro/sup †		$dC_y/d\delta$, lateral head flexion	
	$\alpha = 15°$	$\alpha = 75°$	$\alpha = 15°$	$\alpha = 75°$				
Anchiornis	-0.097 ± 0.003	0.006 ± 0.006	0.239 ± 0.070	0.069 ± 0.013	0.199 ± 0.020	0.330 ± 0.004		
Archaeopteryx	-0.070 ± 0.004	0.010 ± 0.004	0.220 ± 0.071	0.066 ± 0.004	0.420 ± 0.015	0.383 ± 0.016		
Confuciusornis	-0.026 ± 0.002	0.004 ± 0.002	0.002 ± 0.008	-0.004 ± 0.001	0.206 ± 0.025	0.184 ± 0.007		
Jeholornis	-0.091 ± 0.003	0.002 ± 0.001		-0.027 ± 0.007				
Microraptor	-0.100 ± 0.016	0.039 ± 0.010	0.520 ± 0.083	-0.076 ± 0.010	0.259 ± 0.013	0.373 ± 0.008		
Sapeornis	0.002 ± 0.003	0.005 ± 0.001						
Zhongjianornis	0.021 ± 0.003	0.008 ± 0.002	-0.001 ± 0.002	-0.007 ± 0.001	0.296 ± 0.015	0.262 ± 0.015		
Alectoris	0.022 ± 0.001	0.001 ± 0.002	0.019 ± 0.012	-0.050 ± 0.001	0.081 ± 0.013	0.093 ± 0.004		
Buteo	0.027 ± 0.006	-0.002 ± 0.004	-0.007 ± 0.003	-0.029 ± 0.003	0.565 ± 0.060	0.431 ± 0.025		
Columba	0.048 ± 0.002	0.003 ± 0.002	0.005 ± 0.002	-0.022 ± 0.001	0.455 ± 0.042	0.204 ± 0.003		
Larus	0.017 ± 0.004	0.002 ± 0.002		-0.012 ± 0.002				
Onychonycteris	0.025 ± 0.008	-0.040 ± 0.007	-0.011 ± 0.005	-0.012 ± 0.003	0.870 ± 0.093	0.627 ± 0.049		
Pteropus	0.040 ± 0.025	-0.160 ± 0.005						
Pteranodon	0.026 ± 0.002	0.002 ± 0.001			0.271 ± 0.013	0.234 ± 0.004	0.120 ± 0.002	-0.003±0.001
Pterodactylus	-0.002 ± 0.001	0.002 ± 0.001			0.196 ± 0.014	0.139 ± 0.013	0.190 ± 0.003	0.002±0.001
Rhamphorhynchus	-0.052 ± 0.004	-0.034 ± 0.004	0.170 ± 0.008	0.128 ± 0.002	0.279 ± 0.027	0.319 ± 0.024	-0.033±0.009	

*movement depicted in Figure 6D

†movement depicted in Figure 6E

Table S4. Fossil paravians [4] sampled for aerodynamic testing and references used during model construction.

	specimen and reference	approx length $\times 10^{-2}$ m
Anchiornis	LPM B00169 [17]	42
Archaeopteryx	Berlin [23, 18]	40
Confuciusornis	multiple [36]	30
Jeholornis	IVPP V13274, 13553 [37, 38] *	65
Microraptor	IVPP V13352 [16]	85
Sapeornis	IVPP V13275 [39]	27
Zhongjianornis	IVPP V15900 [7]	22

*feathers only in 13553

Table S5. Geometry data for physical models of eight fossil paravians, four extant birds, two bats, three pterosaurs, and two shapes for checking calibration. Aspect ratio calculated as s^2/S.

	area, S $\times 10^{-4}$ m^2	SVL $\times 10^{-2}$ m	TL $\times 10^{-2}$ m	span, s $\times 10^{-2}$ m	AR
Anchiornis	87.11	7.1	18.0	19.6	4.4
Archaeopteryx	94.57	8.0	10.5	17.7	3.4
Confuciusornis	50.53	6.8	9.2	19.9	7.8
Jeholornis	77.03	7.7	19.0	22.7	6.8
Microraptor	114.6	9.3	22.5	19.2	3.2
Sapeornis	54.44	6.6	7.6	20.7	7.8
Zhongjianornis	61.87	8.3	10.1	21.3	7.4
Alectoris	57.89	7.1	9.8	15.0	4.0
Buteo	98.55	8.3	9.9	23.8	5.8
Columba	80.71	7.3	9.8	19.3	4.6
Larus	72.62	7.9	10.5	24.0	8.0
Onychonycteris	194.7	9.6	13.4	29.5	4.4
Pteropus	201.2	8.4	12.4	35.1	6.2
Pteranodon	42.13	6.4	6.5	22.1	11.6
Pterodactylus	51.15	8.4	8.9	19.0	7.0
Rhamphorhynchus	78.56	8.0	18.4	29.7	11.2
Sphere	11.34		3.8	3.8	1.3
Weathervane	39.30		24.0	5.0	0.6